

Unconventional crystal field splitting in non-centrosymmetric BaTiO₃ thin films

Yang Song,^{1,2} Xiaoran Liu,³ Fangdi Wen,³ M. Kareev,³ Ruyi Zhang,^{1,2} Yujuan Pei,^{1,2} Jiachang Bi,^{1,2} Padraic Shafer,⁴ Alpha T. N'Diaye,⁴ Elke Arenholz,⁴ Se Young Park,^{5,6,*} Yanwei Cao,^{1,2,†} and J. Chakhalian³

¹Ningbo Institute of Materials Technology and Engineering,
Chinese Academy of Sciences, Ningbo, Zhejiang 315201, China

²Center of Materials Science and Optoelectronics Engineering,
University of Chinese Academy of Sciences, Beijing 100049, China

³Department of Physics and Astronomy, Rutgers University, Piscataway, New Jersey 08854, USA

⁴Advanced Light Source, Lawrence Berkeley National Laboratory, Berkeley, CA 94720, USA

⁵Center for Correlated Electron Systems, Institute for Basic Science, Seoul 08826, Korea

⁶Department of Physics and Astronomy, Seoul National University, Seoul 08826, Korea

(Dated: January 5, 2022)

Understanding the crystal field splitting and orbital polarization in non-centrosymmetric systems such as ferroelectric materials is fundamentally important. In this study, taking BaTiO₃ as a representative material we investigate titanium crystal field splitting and orbital polarization in non-centrosymmetric TiO₆ octahedra with resonant X-ray linear dichroism at Ti $L_{2,3}$ -edge. The high-quality BaTiO₃ thin films were deposited on DyScO₃ (110) single crystal substrates in a layer-by-layer way by pulsed laser deposition. The reflection high-energy electron diffraction and element specific X-ray absorption spectroscopy were performed to characterize the structural and electronic properties of the films. In sharp contrast to conventional crystal field splitting and orbital configuration ($d_{xz}/d_{yz} < d_{xy} < d_{3z^2-r^2} < d_{x^2-y^2}$ or $d_{xy} < d_{xz}/d_{yz} < d_{x^2-y^2} < d_{3z^2-r^2}$) according to Jahn-Teller effect, it is revealed that d_{xz} , d_{yz} , and d_{xy} orbitals are nearly degenerate, whereas $d_{3z^2-r^2}$ and $d_{x^2-y^2}$ orbitals are split with an energy gap ~ 100 meV in the epitaxial BaTiO₃ films. The unexpected degenerate states $d_{xz}/d_{yz}/d_{xy}$ are coupled to Ti-O displacements resulting from competition between polar and Jahn-Teller distortions in non-centrosymmetric TiO₆ octhedra of BTO films. Our results provide a route to manipulate orbital degree of freedom by switching electric polarization in ferroelectric materials.

I. INTRODUCTION

Ferroelectric materials (oxide films in particular) which exhibit robust spontaneous electric polarization that can be re-oriented with an external electric field, have attracted attention because of their extensive applications such as transistors, memories, and high frequency devices realized in various systems [1–10]. Generally, this spontaneous polarization is coupled to lattice structures such as Ti-O displacements in BaTiO₃ (BTO), a typical ferroelectric material with non-centrosymmetric TiO₆ octahedra [11–14]. Due to crystal field splitting being sensitive to lattice distortions, the ion displacements in ferroelectric materials can modify the crystal field splitting, the study of which is fundamentally important for understanding the properties of ferroelectric materials and non-centrosymmetric superconductors, *e.g.*, the coexistence of superconducting and ferroelectric states in doped perovskite oxides [15, 16], however, crystal field splittings in these system have not been extensively studied yet. [17, 19].

To address the above concern, we take BTO thin films as a representative material to investigate crystal field splitting and orbital polarization in the presence of polar distortions induced by ordering of ferroelectric dipoles. Bulk BaTi⁴⁺O₃ with $3d^0$ electron configuration undergoes complex structural and ferroelectric phase transitions upon cooling, *e.g.*, from high temperature cubic to tetragonal (393 K), tetragonal to orthorhombic (278 K), and orthorhombic to rhombohedral (183 K), where ferroelectric properties are present below 393 K [18, 20, 21]. Moreover, under biaxial compressive strain (such as epitaxial tetragonal BTO films on DyScO₃ substrates) the transition temperature can be enhanced to nearly 500 K and the remnant polarization is at least 2.5 times higher than bulk BTO single crystals [22]. Due to strong *B*-site ferroelectricity at room temperature [23–27], the BTO single crystals are widely used as ferroelectric substrates for epitaxial thin film synthesis [28–30], where its epitaxial films can be employed to manipulate interfacial electric field for controlling order parameters and achieving novel functionalities [31–33].

In this paper, high-quality tetragonal BTO thin films were grown on DyScO₃ (DSO) (110) single crystal substrates

* sp2829@snu.ac.kr

† ywcao@nimte.ac.cn

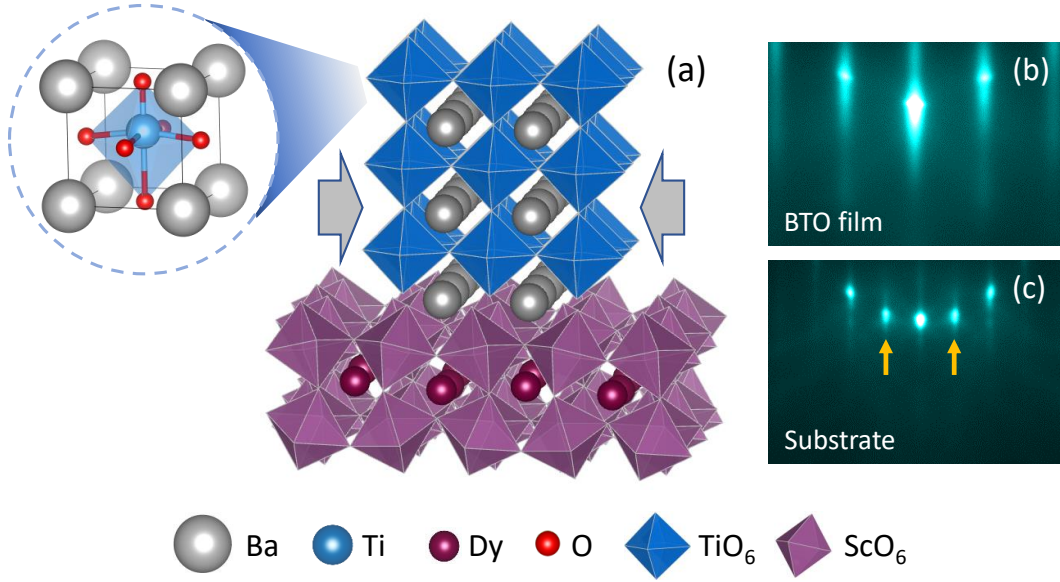


FIG. 1. (a) Schematic of epitaxial BTO film on a DSO substrate. The two arrows indicate biaxial compressive strain on BTO film. (b-c) RHEED patterns of (b) BTO film (after growth at room temperature) and (c) DSO (110) substrate (before growth). The yellow arrows indicate the half-order Bragg peaks.

in a layer-by-layer way by pulsed laser deposition (PLD). The structural and electronic properties were characterized by reflection high-energy electron diffraction (RHEED) and element-specific X-ray absorption spectroscopy (XAS). In sharp contrast to conventional crystal field splitting and orbital polarization from the Jahn-Teller effect, an anomalous orbital structure, nearly degenerate t_{2g} ($d_{xz}/d_{yz}/d_{xy}$) and split e_g ($d_{3z^2-r^2} < d_{x^2-y^2}$ about 100 meV) orbitals, was revealed in epitaxial BTO films, resulting from the competition between polar and Jahn-Teller distortions in non-centrosymmetric TiO_6 octhedra of polar BTO films.

II. EXPERIMENTS AND FIRST-PRINCIPLES CALCULATIONS

As shown in Fig. 1, the BTO films (20 unit cells, ~ 8.2 nm) had been grown along [110] (orthorhombic notation, corresponding to [001] orientation in a pseudocubic notation) DSO substrates ($5 \times 5 \times 0.5 \text{ mm}^3$) by PLD, using a KrF excimer laser operating at $\lambda = 248 \text{ nm}$ and 2 Hz pulse rate with 2 J/cm^2 fluence. During the growth, the oxygen pressure was kept at $\sim 10^{-6}$ Torr, the temperature of the substrates was $\sim 850^\circ\text{C}$ (from reader of infrared pyrometers). At room temperature, the bulk lattice parameters are $a = 3.99 \text{ \AA}$ and $c = 4.04 \text{ \AA}$ for tetragonal BTO, and $a = 3.95 \text{ \AA}$ for DSO (pseudo cubic). Due to the lattice mismatch, the epitaxial BTO films

on DSO are under biaxial compressive strain, indicated by a pair of arrows in Fig. 1(a). In order to monitor the growth of the BTO thin film, an *in-situ* RHEED was performed during the deposition. The sharp RHEED patterns, Fig. 1(b) and (c), suggest a high-quality two-dimensional growth of the BTO films. In order to investigate the electronic structure of BTO films, linearly polarized XAS in luminescence yield detection mode (bulk-sensitive, see Fig. 2(a)) was performed at room temperature at beamline 4.0.2 of the Advanced Light Source (ALS, Lawrence Berkeley National Laboratory) [34], and the preliminary data were collected at beamline 6.3.1. We have carried out first-principles density-functional theory (DFT) calculations within the local density approximation (LDA) [35, 36]. The calculations are performed using the Vienna *ab-initio* simulation package (VASP) [37, 38]. The projector augmented wave (PAW) [39] is used with an energy cut-off of 600 eV. The Brillouin zone is sampled with a $8 \times 8 \times 8$ k -point grid for 5-atom unit cell of BTO. Convergence is reached if the consecutive energy difference is less than 10^{-6} eV for electronic iterations and 10^{-5} eV for ionic relaxations. The polarization is calculated using the Berry-phase method [40] as implemented in VASP. The tight-binding parameters for Ti d -orbitals are calculated by Wannier90 package [41].

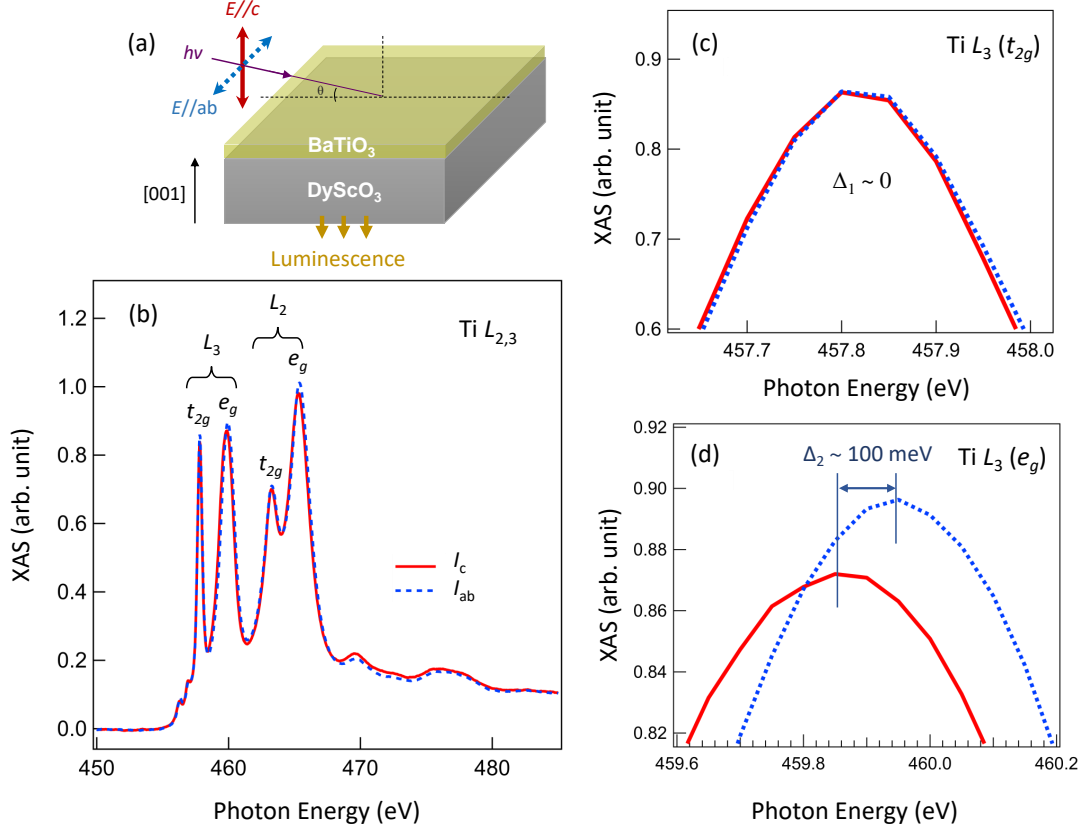


FIG. 2. (a) Schematic of experimental setup. $E \parallel c$ and $E \parallel ab$ (E is the polarization vector of the photon) indicate out-of-plane (red solid line, I_c) and in-plane (blue dash line, I_{ab}) linearly polarized incident X-ray, respectively. The grazing angle $\theta = 20^\circ$. The yellow arrows at the bottom of DSO substrates indicates the bulk-sensitive luminescence yield detection mode. The arrow along $[001]$ direction (pseudocubic notation) indicates the growth direction of BTO films. (b) XAS of BTO films at Ti $L_{2,3}$ -edge at room temperature. All collected spectra are repetitively measured more than six times. Enlarged XAS spectra at (c) Ti L_3 (t_{2g}) and (d) Ti L_3 (e_g) absorption peaks. Δ_1 and Δ_2 are defined as the splitting between d_{xy} and d_{xz}/d_{yz} orbitals, and between $d_{x^2-y^2}$ and $d_{3z^2-r^2}$ orbitals, respectively

III. RESULTS AND DISCUSSIONS

Figure 2(b) shows the XAS spectra of BTO films at Ti $L_{2,3}$ -edge. There are four well split characteristic peaks, arising from the excitations from Ti $2p$ to Ti $3d$ states (the electronic configuration changes from Ti $2p^6 3d^0$ to $2p^5 3d^1$). Generally, in octahedral symmetry, the transition-metal d bands split into t_{2g} (d_{xy} , d_{xz} , d_{yz}) and e_g ($d_{3z^2-r^2}$, $d_{x^2-y^2}$) [42–48]. The degenerate t_{2g} and e_g bands further split when the octahedron experiences uniaxial elongation or compression [49], along the c -axis where the Jahn-Teller distortion leads to orbital structure $d_{xz}/d_{yz} < d_{xy} < d_{3z^2-r^2} < d_{x^2-y^2}$ or $d_{xy} < d_{xz}/d_{yz} < d_{x^2-y^2} < d_{3z^2-r^2}$, respectively. Using that intensity of linearly polarized XAS carries the information of crystal field splitting and orbital polarization [42–48], Fig. 2(c) and (d) show the differences between out-of-plane (I_c) and in-plane (I_{ab}) polarized XAS. As seen in the figure, the t_{2g} or-

bitals are nearly degenerate ($\Delta_1 \sim 0$, see Fig. 2(c)), whereas the splitting Δ_2 between $d_{x^2-y^2}$ and $d_{3z^2-r^2}$ orbitals in e_g state is about 100 meV, shown in Fig. 2(d). The same orbital splitting is observed at Ti L_2 -edge as well. This kind of orbital structure in BTO films ($d_{xz}/d_{yz}/d_{xy} < d_{3z^2-r^2} < d_{x^2-y^2}$) is unexpected and in sharp contrast to conventional crystal field splitting ($d_{xz}/d_{yz} < d_{xy} < d_{3z^2-r^2} < d_{x^2-y^2}$) in elongated TiO_6 octahedra along the c axis [50].

To further understand this anomalous orbital structure in BTO films, we obtain the spectra of X-ray linear dichroism (XLD), which is defined as $\text{XLD} = I_c - I_{ab}$ in this work. Figure 3 shows the XLD spectra of the biaxial compressive BTO and CaTiO_3 (CTO) films at Ti $L_{2,3}$ -edge. We note that among ATiO_3 titanates ($A = \text{Ba}, \text{Sr}, \text{Ca}$) only *without* Ti-O displacements from the center of TiO_6 octahedra are taken as a reference material to compare with ferroelectric BTO films *with* Ti-O displacements. As highlighted in the orange area in Fig. 3,

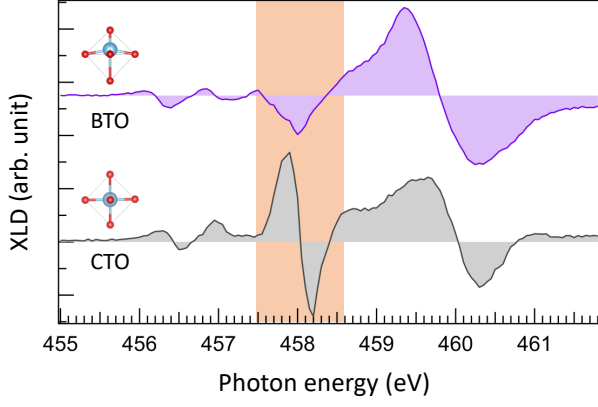


FIG. 3. XLD of BTO (in purple, with Ti-O displacements) and CTO (in gray, without Ti-O displacements) [50] thin films at room temperature. The rectangular orange shadow highlights the contribution of ferroelectric polarization on crystal field splitting and orbital polarization.

the XLD of CTO indicates crystal field splitting ($d_{xz}/d_{yz} < d_{xy}$) within t_{2g} states, whereas t_{2g} orbitals are nearly degenerate ($d_{xz}/d_{yz}/d_{xy}$) in BTO films.

The discrepancy between the degenerate t_{2g} orbitals and the expected crystal field splitting from the compressive strain strongly suggest an additional mechanism behind unusual orbital splitting. Since the bulk BTO is ferroelectric at room temperature [18], it is natural to include the polar distortion in BTO and investigate its contribution to the orbital splitting. Using the first-principles DFT method, we first calculate the effect of the epitaxial strain on the Jahn-Teller distortion (or change in the c/a ratio) without considering the polar distortion. With 1.25% compressive strain based on the lattice mismatch between BTO and DSO, the c/a ratio obtained by strained-bulk calculation increases to 1.02. Next, we allow a polarization along the c -axis, experimentally observed under the compressive strain [51]. The relaxed atomic structure with 1.25% compressive epitaxial strain lowers the total energy by 19 meV per formula unit from a polar distortion, mainly contributed by Ti displacement from the center of the octahedron with Ti-O-Ti angle of 172° . The calculated polarization is $33 \mu\text{C}/\text{cm}^2$ along the c axis with further increase in the c/a ratio to 1.04.

In order to investigate the effect of the Jahn-Teller and polar distortion to orbital polarization, we consider two atomic configurations: one with Jahn-Teller distortion with $c/a = 1.04$ with zero polar distortion and the other with cubic lattice constant of 1.25% compressive strain for all the lattice constant including polar distortion of the strained bulk calculation. The projected density of states (PDOS) and Wannier tight-binding

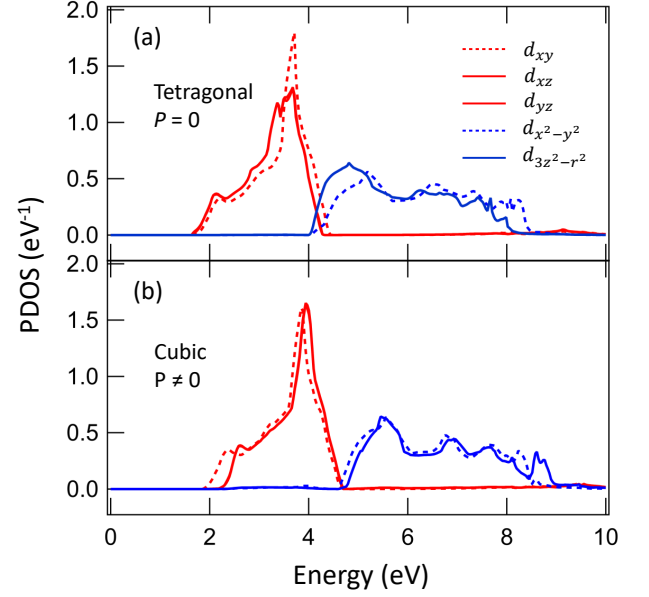


FIG. 4. PDOS of the strained bulk calculations with 1.25% biaxial compressive strain. PDOS of (a) tetragonal BTO with zero polarizations ($c/a = 1.04$) and (b) cubic BTO with polar distortion.

parameters are presented in Fig. 4 and table I, respectively. In Fig. 4(a), we find that the effect of the Jahn-Teller distortion from the compressive strain is straightforwardly shown in the PDOS with $d_{xz}/d_{yz} < d_{xy}$ and $d_{3z^2-r^2} < d_{x^2-y^2}$ orbital splitting, consistent with on-site energy difference $E_{xz/yz} - E_{xy} = -0.13 \text{ eV}$ for t_{2g} orbitals and $E_{3z^2-r^2} - E_{x^2-y^2} = -0.45 \text{ eV}$ for e_g orbitals (Table I). We note that the splitting between t_{2g} orbitals is smaller than that of e_g orbitals due to the relatively weaker π bonding of t_{2g} orbitals compared to the σ bonding of e_g . In contrast, the inclusion of the polar distortion without considering the Jahn-Teller distortion results in the opposite trend in the PDOS as shown in Fig. 4(b): $d_{xz}/d_{yz} > d_{xy}$ and $d_{3z^2-r^2} > d_{x^2-y^2}$ orbital splitting, consistent with the on-site energy difference of $E_{xz/yz} - E_{xy} = 0.15 \text{ eV}$ for t_{2g} orbitals and of $E_{3z^2-r^2} - E_{x^2-y^2} = 0.13 \text{ eV}$ for e_g orbitals (Table I). We note that the splitting between the t_{2g} orbitals from the polar distortion is larger than that between e_g orbitals, consistent with relatively larger reduction in the in-plane hopping $t_{xz/yz}^{\parallel}$ about 50 meV than that of $t_{x^2-y^2}^{\parallel}$ about 20 meV compared with the cubic hopping parameters. This suggests that the bonding between the t_{2g} orbitals is more sensitive to the Ti-O-Ti angle than that between the e_g orbitals.

From the opposite tendencies of the orbital splitting between the Jahn-Teller and polar distortions, we can understand the orbital polarization observed in the XLD measurements; the degeneracy of the t_{2g} orbitals is maintained by the cancellation of orbital splitting from Jahn-Teller and polar distortion.

TABLE I. On-site energies and major hopping parameters of Ti d -orbital for BTO (in eV) obtained from Wannier functions of Ti d -band. For hopping parameter t , \parallel and \perp represent the in-plane and out-of-plane hopping, respectively.

	On-site energy difference		Intra orbital hopping				
	$E_{xz/yz} - E_{xy}$	$E_{3z^2-r^2} - E_{x^2-y^2}$	t_{xy}^{\parallel}	$t_{xz/yz}^{\parallel}$	$t_{xz/yz}^{\perp}$	$t_{x^2-y^2}^{\parallel}$	$t_{3z^2-r^2}^{\perp}$
Cubic	0	0	-0.31	-0.31	-0.31	-0.50	-0.66
Tetragonal ($P = 0$)	-0.13	-0.45	-0.30	-0.33	-0.25	-0.50	-0.64
Cubic ($P \neq 0$)	0.15	0.13	-0.30	-0.26	-0.28	-0.48	-0.66

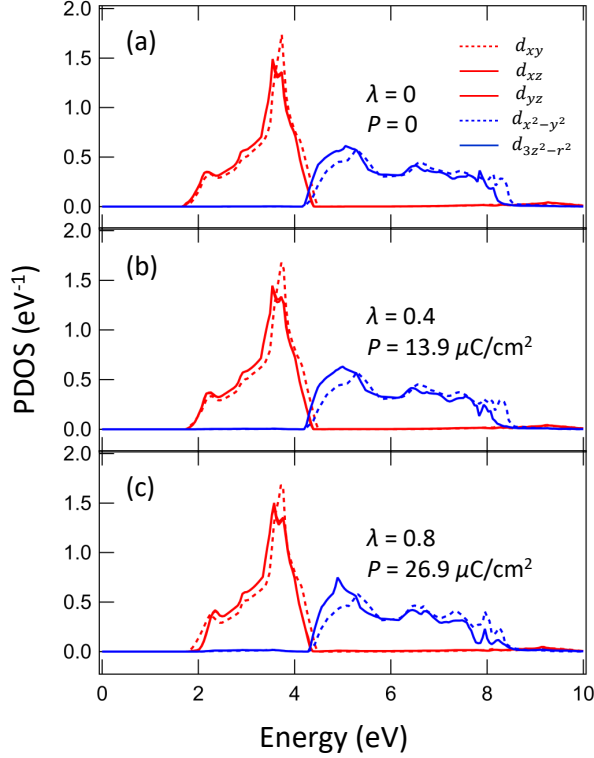


FIG. 5. PDOS of the atomic structures linearly interpolated between non-polar strained bulk BTO structure with $c/a = 1.02$ and polar strained bulk BTO structure with $P = 33 \mu\text{C}/\text{cm}^2$. The symbol λ is defined as the parameter of the linear interpolation ($\lambda = 0$ and 1 for non-polar and polar structures). PDOS for (a) $\lambda = 0$, (b) $\lambda = 0.4$ ($P = 14 \mu\text{C}/\text{cm}^2$) and (c) $\lambda = 0.8$ ($P = 27 \mu\text{C}/\text{cm}^2$).

tions which are similar in amount (-0.13 eV vs 0.15 meV), while the degeneracy of e_g orbitals is lifted due to larger difference of the orbital splitting from the Jahn-Teller and polar distortions (-0.45 eV vs 0.13 eV). To confirm this idea, we calculate the PDOS of the structures obtained by linear interpolation between the strained bulk atomic structure without polarization ($c/a = 1.02$) parameterized by $\lambda = 0$ and strained bulk atomic structure with out-of-plane polarization ($c/a = 1.04$) parameterized by $\lambda = 1$. Fig. 5 shows the PDOS with $\lambda = 0, 0.4$, and 0.8 . For the all values of the λ ,

the splitting of the e_g orbital is maintained due to the splitting from the elongated c -axis ($c/a > 1.02$) dominating the e_g orbital splitting. In contrast, the sign change in the t_{2g} orbital splitting is clearly seen for $\lambda = 0$ and $\lambda = 0.8$. In particular, for $\lambda = 0.4$, the t_{2g} orbitals are closely degenerate while e_g orbitals split about 0.3 eV , consistent with the experimental data. For the $\lambda = 0.4$, the polarization value reduced to about 42% of the $\lambda = 1$ structure, which may come from the finite thickness of BTO, suppressing the polarization.

We compare the crystal-field-induced splitting between polar BTO without octahedral rotation and tilts and non-polar CaTiO_3 (CTO) with $a^-a^-c^+$ octahedral rotation and tilts commonly observed in perovskite oxides, illustrated in Fig. 6. For TiO_6 octahedra under biaxial compressive strain, the orbital structure ($d_{xz}/d_{yz} < d_{xy} < d_{3z^2-r^2} < d_{x^2-y^2}$) in biaxial compressive CTO films is expected due to elongated Ti-O bonds along the c -axis. With combined tetragonal and polar distortions in BTO, a large orbital splitting between e_g orbitals ($d_{3z^2-r^2} < d_{x^2-y^2}$) with an energy gap about 100 meV is observed from the dominated Jahn-Teller splitting from increased c/a ratio, whereas t_{2g} ($d_{xz}/d_{yz}/d_{xy}$) orbitals are nearly degenerate in the BTO thin film from the competition between polar and Jahn-Teller distortions. The unusual orbital structure we have observed in this work may provide a clue to understand the peculiar band splitting of BTO investigated by angle-resolved photoemission spectroscopy (ARPES) [52], by including the crystal field splitting from polar distortions. Our finding here provides an effective way to manipulate orbital degree of freedom by manipulating ferroelectric polarization which could be used to design exotic quantum states, such as metal-insulator transition, superconductivity, and colossal magneto-resistance.

IV. CONCLUSION

In summary, we have synthesized high-quality BTO thin films on DSO substrates with a layer-by-layer growth by PLD and characterized their structural and electronic properties by

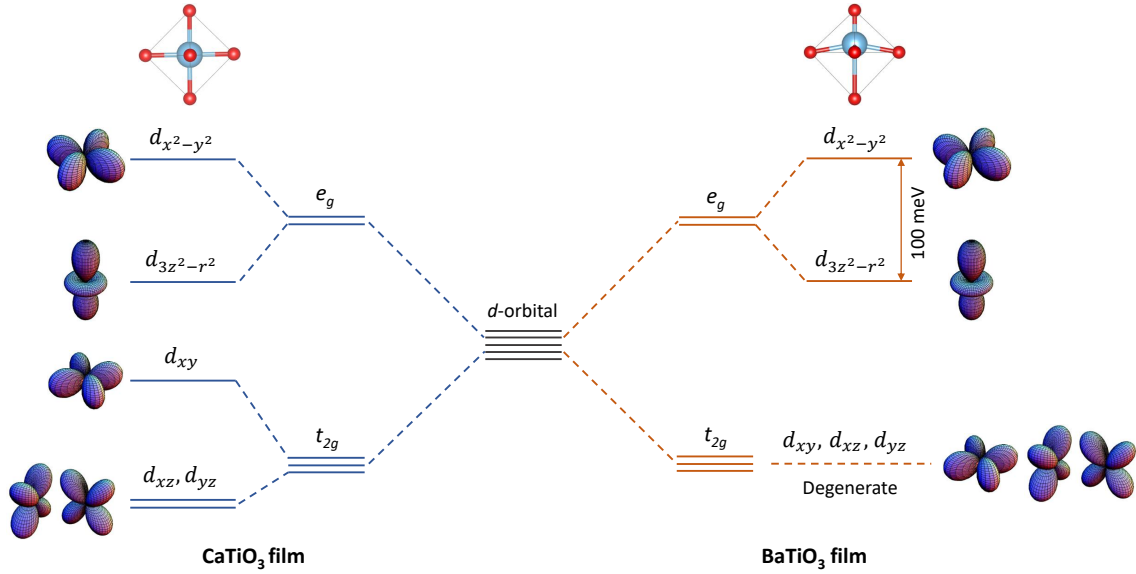


FIG. 6. Contrastive crystal field splitting of CTO films (left panel, without Ti-O displacements) and BTO films (right panel, with Ti-O displacements).

RHEED, element-specific XAS/XLD, and DFT calculation. In sharp contrast to conventional crystal field splitting and orbital configuration ($d_{xz}/d_{yz} < d_{xy} < d_{3z^2-r^2} < d_{x^2-y^2}$) in elongated TiO₆ octahedra such as compressive CTO films, the XLD spectra reveals that the orbital structure in BTO films is unconventional: nearly degenerate t_{2g} ($d_{xz}/d_{yz}/d_{xy}$) and split e_g ($d_{3z^2-r^2} < d_{x^2-y^2}$ with a gap ~ 100 meV) states. The first-principles DFT calculations show that this unexpected degenerate t_{2g} orbitals are from the competition between polar and Jahn-Teller distortions in the non-centrosymmetric TiO₆ octahedra of BTO films. Our work could pave a way to design exotic quantum states (such as tunable multiferroic properties) by manipulating the orbital degree of freedom using the switchable ferroelectric polarizations.

ACKNOWLEDGMENTS

We acknowledge insightful discussions with Darren C. Peets. This work is supported by the National Natural Science Foundation of China (Grant No. 11874058), the Pioneer Hundred Talents Program of the Chinese Academy of Sciences, the Ningbo 3315 Innovation Team, and the Ningbo Science and Technology Bureau (Grant No. 2018B10060). J. C. acknowledges support from the Gordon and Betty Moore Foundation EPiQS Initiative through Grant No. GBMF4534. This research used resources of the Advanced Light Source, which is a DOE Office of Science User Facility under contract No. DE-AC02-05CH11231. S. P. acknowledges support from the Institute for Basic Science in Korea (Grant No. IBS-R009-D1).

-
- [1] L. W. Martin and A. M. Rappe, Nat. Rev. Mater. **2**, 16087 (2016).
 - [2] R. Resta, Rev. Mod. Phys. **66**, 899 (1994).
 - [3] M. Dawber, K. M. Rabe, and J. F. Scott, Rev. Mod. Phys. **77**, 1083 (2005).
 - [4] D. G. Schlom, L. Q. Chen, C. B. Eom, K. M. Rabe, S. K. Streiffer, and J. M. Triscone, Annu. Rev. Mater. Res. **37**, 589 (2007).
 - [5] N. Setter, D. Damjanovic, L. Eng, G. Fox, S. Gevorgian, S. Hong, A. Kingon, H. Kohlstedt, N. Y. Park, G. B. Stephenson, I. Stolitchnov, A. K. Taganov, D. V. Taylor, T. Yamada, and S. Streiffer, J. Appl. Phys. **100**, 051606 (2006).
 - [6] R. Ramesh and N. A. Spaldin, Nat. Mater. **6**, 21 (2007).
 - [7] W. Eerenstein, N. D. Mathur, and J. F. Scott, Nature **442**, 759 (2006).
 - [8] R. E. Cohen, Nature **358**, 136 (1992).
 - [9] N. A. Spaldin and M. Fiebig, Science **309**, 391 (2005).
 - [10] W. Yun, J. Urban, Q. Gu, and H. Park, Nano Lett. **2**, 447 (2002).
 - [11] H. N. Lee, H. M. Christen, M. F. Chisholm, C. M. Rouleau, and D. H. Lowndes, Nature **433**, 395 (2005).
 - [12] H. Guo, Z. Wang, S. Dong, S. Ghosh, M. Saghayezhian, L. Chen, Y. Weng, A. Herklotz, T. Z. Ward, R. Jin, S. T. Pantelides, Y. Zhu, J. Zhang, and E. W. Plummer, Proc. Natl. Acad. Sci.

- U.S.A. **114**, E5062 (2017).
- [13] Y. Cao, Z. Wang, S. Y. Park, Y. Yuan, X. Liu, S. M. Nikitin, H. Akamatsu, M. Kareev, S. Middey, D. Meyers, P. Thompson, P.J. Ryan, P. Shafer, A. NDiaye, E. Arenholz, V. Gopalan, Y. Zhu, K. M. Rabe, and J. Chakhalian, *Nat. Commun.* **9**, 1547 (2018).
 - [14] F. Cordero, F. Trequattrini, F. Craciun, H. Langhammer, D. Quiroga, and P. Silva Jr. *Phys. Rev. B* **99**, 064106 (2019).
 - [15] M. Gabay and J.-M. Triscone. *Nat. Phys.* **13**, 624, (2017).
 - [16] C. W. Rischau, X. Lin, C. P. Grams, D. Finck, S. Harms, J. Engelmayer, T. Lorenz, Y. Gallais, B. Fauqu, J. Hemberger, and K. Behnia. *Nat. Phys.* **13**, 643, (2017).
 - [17] C. Schmitz-Antoniak, D. Schmitz, P. Borisov, F. de Groot, S. Stienen, A. Warland, B. Krumme, R. Feyerherm, E. Dudzik, W. Kleemann, and H. Wende, *Nat. Commun.* **4**, 2051 (2013).
 - [18] G.H. Kwei, A. C. Lawson, S. J. L. Billinge and S.-W. Cheong, *J. Phys. Chem.* **97** 2368 (1993)
 - [19] E. Arenholz, G. Van der Laan, A. Fraile-Rodriguez, P. Yu, Q. He, and R. Ramesh, *Phys. Rev. B* **82**, 140103 (2010).
 - [20] T. Ishidate, S. Abe, H. Takahashi, and N. Môri, *Phys. Rev. Lett.* **78**, 2397 (1997).
 - [21] S. A. Hayward and E. K. H. Salje, *J. Phys.: Condens. Matter* **14**, L599 (2002).
 - [22] K. Choi, M. Biegalski, Y. Li, A. Sharan, J. Schubert, R. Uecker, P. Reiche, Y. Chen, X. Pan, V. Gopalan, L. Chen, D. Schlom, and C. Emo, *Science* **306**, 1005 (2004).
 - [23] M. B. Smith, K. Page, T. Siegrist, P. L. Redmond, E. C. Walter, R. Seshadri, L. E. Brus, and M. L. Steigerwald, *J. Am. Chem. Soc.* **130**, 6955 (2008).
 - [24] C. Ma, K. Jin, C. Ge, and G. Yang, *Phys. Rev. B* **97**, 115103 (2018).
 - [25] P. Blom, R. Wolf, J. Cillessen, and M. Krijn, *Phys. Rev. Lett.* **73**, 2107 (1994).
 - [26] A. Kholkin, E. Colla, A. Tagantsev, D. Taylor, and N. Setter, *Appl. Phys. Lett.* **68**, 2577 (1996).
 - [27] C. Ma, X. He, and K. Jin, *Phys. Rev. B* **96**, 035140 (2017).
 - [28] A. Alberca, C. Munuera, J. Tornos, F. Mompean, N. Biskup, A. Ruiz, N. Nemes, A. de Andres, C. Len, J. Santamara and M. Garca-Hernandez. *Phys. Rev. B* **86**, 144416 (2012).
 - [29] S. Brivio, D. Petti, R. Bertacco, and J. Cezar. *Appl. Phys. Lett.* **98**, 092505 (2011).
 - [30] M. Lee, T. Nath, C. Eom, M. Smoak, and F. Tsui. *Appl. Phys. Lett.* **77**, 3547-3549 (2000).
 - [31] L. Wang, Q. Feng, Y. Kim, R. Kim, K. H. Lee, S. D. Pollard, Y. J. Shin, H. Zhou, W. Peng, D. Lee, W. Meng, H. Yang, J. H. Han, M. Kim, Q. Lu, and T. W. Noh. *Nat. Mater.* **17**, 1087, (2018).
 - [32] B. Cui, C. Song, H. Mao, Y. Yan, F. Li, S. Gao, J. Peng, F. Zeng, and F. Pan, *Adv. Funct. Mater.* **26**, 753 (2016).
 - [33] K. Takahashi, Y. Matsubara, M. Bahramy, N. Ogawa, D. Hashizume, Y. Tokura, and M. Kawasaki. *Scientific reports* **7**, 4631 (2017).
 - [34] Y. Cao, P. Shafer, X. Liu, D. Meyers, M. Kareev, S. Middey, J. Freeland, E. Arenholz, and J. Chakhalian. *Appl. Phys. Lett.* **107**, 112401 (2015).
 - [35] D. M. Ceperley and B. J. Alder, *Phys. Rev. Lett.* **45**, 566 (1980).
 - [36] J. P. Perdew and A. Zunger, *Phys. Rev. B* **23**, 5048 (1981).
 - [37] G. Kresse and J. Furthmüller, *Phys. Rev. B* **54**, 11169 (1996).
 - [38] G. Kresse, and D. Joubert, *Phys. Rev. B* **59**, 1758 (1999).
 - [39] P. E. Blöchl, *Phys. Rev. B* **50**, 17953 (1994).
 - [40] R. D. King-Smith and D. Vanderbilt, *Phys. Rev. B* **47**, 1651 (1993)
 - [41] A. A. Mostofi, J. R. Yates, G. Pizzi, Y.-S. Lee, I. Souza, D. Vanderbilt, and N. Marzari, *Comp. Phys. Commun.* **185**, 2309 (2014).
 - [42] J. S. Lee, Y. W. Xie, H. K. Sato, C. Bell, Y. Hikita, H. Y. Hwang, and C. C. Kao, *Nat. Mater.* **12**, 703 (2013).
 - [43] M. Salluzzo, J. C. Cezar, N. B. Brookes, V. Bisogni, G. M. De Luca, C. Richter, S. Thiel, J. Mannhart, M. Huijben, A. Brinkman, G. Rijnders, and G. Ghiringhelli, *Phys. Rev. Lett.* **102**, 166804 (2009).
 - [44] M. Salluzzo, S. Gariglio, D. Stornaiuolo, V. Sessi, S. Rusponi, C. Piamonteze, G. M. De Luca, M. Minola, D. Marré, A. Gadaleta, H. Brune, F. Nolting, N. B. Brookes, and G. Ghiringhelli, *Phys. Rev. Lett.* **111**, 087204 (2013).
 - [45] M. Salluzzo, S. Gariglio, X. Torrelles, Z. Ristic, R. Di Capua, J. Drnec, M. Moretti Sala, G. Ghiringhelli, R. Felici, and N. B. Brookes, *Adv. Mater.* **25**, 2333 (2013).
 - [46] D. Pesquera, M. Scigaj, P. Gargiani, A. Barla, J. Herrero-Martín, E. Pellegrin, S. M. Valvidares, J. Gázquez, M. Varela, N. Dix, J. Fontcuberta, F. Sánchez, and G. Herranz, *Phys. Rev. Lett.* **113**, 156802 (2014).
 - [47] Y. Cao, Z. Yang, M. Kareev, X. Liu, D. Meyers, S. Middey, D. Choudhury, P. Shafer, J. Guo, J. W. Freeland, E. Arenholz, L. Gu, and J. Chakhalian, *Phys. Rev. Lett.* **116**, 076802 (2016).
 - [48] Y. Cao, X. Liu, P. Shafer, S. Middey, D. Meyers, M. Kareev, Z. Zhong, J.W. Kim, P. Ryan, E. Arenholz, and J. Chakhalian, *npj Quantum Mater.* **1**, 16009 (2016).
 - [49] D. Louca, T. Egami, E. Brosha, H. Rder, and A. Bishop, *Phys. Rev. B* **56**, R8475 (1997).
 - [50] Y. Cao, S. Park, X. Liu, D. Choudhury, S. Middey, D. Meyers, M. Kareev, P. Shafer, E. Arenholz, and J. Chakhalian, *Appl. Phys. Lett.* **109**, 152905 (2016).
 - [51] Oswaldo Dieguez, Silvia Tinte, A. Antons, Claudia Bungaro, J. B. Neaton, Karin M. Rabe, and David Vanderbilt, *Phys. Rev. B* **69**, 212101 (2004).
 - [52] T. Rdel, M. Vivek, F. Fortuna, P. Le Fvre, F. Bertran, R. Weht, J. Goniakowski, M. Gabay, and A. Santander-Syro. *Phys. Rev. B* **96**, 041121 (2017).